Journal of Alloys and Compounds 509 (2011) 5336–5340

Contents lists available at ScienceDirect

Journal of Alloys and Compounds

journal homepage: www.elsevier.com/locate/jallcom

Enhancement of the upconversion luminescence intensity in Er^{3+} doped $BaTiO_3$ nanocrystals by codoping with Li^+ ions

Qiu Sun [a], Xiangqun Chen [b,*], Zhikai Liu [b], Fuping Wang [a], Zhaohua Jiang [a], Chao Wang [c]

[a] School of Chemical Engineering and Technology, Harbin Institute of Technology, Harbin 150001, People's Republic of China
[b] Department of Material Physics and Chemistry, School of Materials Science and Engineering, Harbin Institute of Technology, Harbin 150001, People's Republic of China
[c] Institute of Petrochemistry, Heilongjiang Academy of Sciences, Harbin 150040, People's Republic of China

ARTICLE INFO

Article history:
Received 24 November 2010
Received in revised form
27 December 2010
Accepted 30 December 2010
Available online 17 February 2011

Keywords:
Luminescence
Oxygen vacancy
Local asymmetry
Decay time

ABSTRACT

Infrared-to-visible upconversion luminescence spectra were investigated in Er^{3+} doped and Er^{3+}–Li^+ codoped $BaTiO_3$ nanocrystals following excitation with 976 nm. By introducing Li^+ ions, the upconverted emission intensity is found to be greatly enhanced compared to that of the nanocrystals without Li^+ ions. The enhanced luminescence might be attributed to the oxygen vacancy generated by Li^+ ion incorporation in the lattices and the distortion of the local asymmetry around Er^{3+}. We observe that excitation power dependence and decay time are increased by the incorporation of Li^+ ions. Li^+ ions also can reduce the OH groups in specimen, which decrease nonradiative decay from the $^4S_{3/2}$ to $^4F_{9/2}$, enhancing the upconversion emission intensities.

1. Introduction

Rare-earth (RE) doped materials have attracted much research interest due to their potential applications such as volumetric displays, temperature sensors, upconversion (UC) lasers, biomedical imaging, DNA detection, and photodynamic therapy [1–5]. With a suitable selection of the host matrix and the rare earth dopant ion concentration, the UC performance of a material can be enhanced significantly. Numerous host matrixes, such as $NaYF_4$, Y_2O_3, Gd_2O_3, ZrO_2, have been investigated as host matrix for UC phosphors due to their relatively low phonon cutoff energy [6–9]. $BaTiO_3$ (BTO) is suitable for host matrix as UC phosphors because of its good properties, such as its low phonon energy (about 700 cm^{-1}), good insulating property, and its chemical and physical stability. Up to now, some reports dealing with UC luminescence properties of BTO nanoparticles have been presented [10]. For instance, Patra et al. prepared BTO: Er^{3+} by sol–emulsion–gel method, and studied their UC fluorescence properties [11]. Zhang et al. prepared Er-doped BTO nanocrystalline films with sol–gel method, and discussed the green UC luminescence of the films [12]. Among these rare earth ions, the erbium ion is the most popular as well as one of the most efficient ions for UC luminescence because the meta stable levels $^4I_{9/2}$ and $^4I_{11/2}$ of Er^{3+} can be conveniently populated by commercial low-cost high-power 800 nm and 980 nm laser diodes, respectively [13–16]. Realization of efficient NIR to visible UC in BTO nanocrytals will have great impact on deploying their potential advantages.

However, the intensity of UC emission of RE-doped BTO is lower than that of RE compounds as matrix. It is, therefore, of great interest to further significantly increase the UC emission in the Er^{3+} doped BTO nanocrystals. According to the quantum mechanical selection rules, the main intra-4f electronic-dipole transitions of rare-earth ions are forbidden, which can be broken by the local crystal field of the rare-earth ions due to the capability to intermix their f states with higher electronic configurations. Hence, the tailoring rare-earth ions' local environment in the host lattice is a promising route to enhance their optical performance. Chen et al. have reported greater enhancement of the visible UC radiation in different nanocrystals by doping with Li^+ ions [17,18]. Bai et al. have found that the green emission intensity is greatly enhanced with 2 mol% Li^+ doping in ZnO/Er^{3+} nanocrystals [19]. The reasons for the enhancement are attributed to the decrease of the local symmetry around the Er^{3+} ion and the reducing OH groups of UC materials. As a promising UC emission matrix materials, $BaTiO_3$ has the typical configuration of ABO_3. Until now, few authors have observed the effect of Li^+ ions on upconversion emission of Er^{3+}-doped ABO_3 materials. Here we report on a 27 times enhancement of the visible UC radiation in $BaTiO_3$: 1Er nanocrystals and 56 times in $BaTiO_3$: 2Er by codoping with Li^+.

* Corresponding author at: Department of Material Physics and Chemistry, School of Materials Science and Engineering, Harbin Institute of Technology, No. 92, West Da-Zhi Street, Harbin 150001, People's Republic of China. Tel.: +86 45186418409.
E-mail address: chenxq@hit.edu.cn (X. Chen).

0925-8388/$ – see front matter © 2011 Elsevier B.V. All rights reserved.
doi:10.1016/j.jallcom.2010.12.212

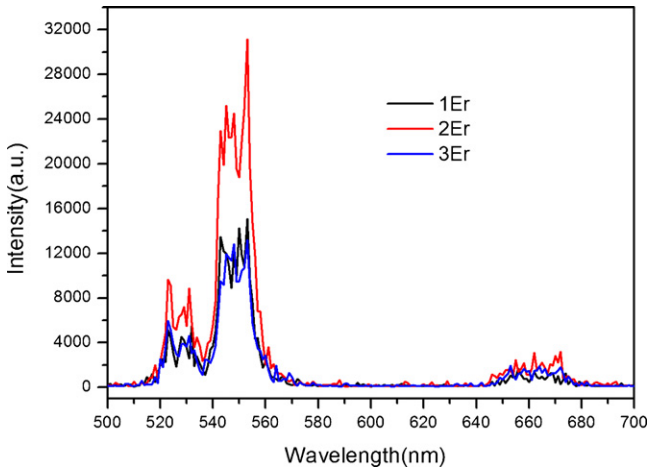

Fig. 1. NIR-to-visible upconversion emission spectra of BTO doped with 1, 2, and 3 mol% Er^{3+} ions under 976 nm laser excitation.

2. Experimental

2.1. Preparation of BTO: 1%Er2%Li (BTO: 1Er2Li) nanoparticles

For the synthesis of BTO: 1Er2Li, $Ba(CH_3COO)_2$ (3.678 g, and 14.55 mmol), $Er(NO_3)_3{\cdot}6H_2O$ (71.1 mg, and 0.15 mmol) and $LiNO_3$ (0.021 mg, and 0.3 mmol) were dissolved in 10 mL water followed by adding 10 mL acetic acid and 10 mL ethanol. Required amounts of acetic acid (5 mL) and ethol (20 mL) were mixture. Next, $Ti(OC_4H_9)_4$ (5 mL) was added to the mixture of acetic acid and ethanol to form the titania sol. The titania sol was added dropwise into the solution of $Ba(CH_3COO)_2$, under vigorous stirring at ambient temperature. A yellow transparent sol obtained formed a gel over an hour at 80 °C, and then the gel was dried at 120 °C for 5 h. The resulting sol–gel precursor powders were calcined at 800 °C for 2 h to obtain the final powders.

2.2. Characterization

WAXD pattern was obtained for the powder specimen on a D/max-γB X-ray diffractometer using a graphite monochromator CuKα radiation (40 kV, λ = 0.1546 nm). The scanning rate was 0.02°/min over a range of 2θ = 10–80°. Fourier transform infrared (FT-IR) spectra were measured with a Nicolet-Nexus 670 infrared spectrometer via the potassium bromide (KBr) pellet technique. In making the KBr pelletes, 2 mg of sample after heated 110 °C for 2 h was mixed with 100 mg of KBr powder. Further, the powders were pressed to form smooth and flat disks to be utilized for UC spectral studies. The focus area on the disk sample was measured to be about 1 mm^2. Samples were irradiated with a controllable-power 976 nm diode laser (Hi-Tech Optoelectronics Co., Ltd., Beijing) with the maximum output power of 500 mW. The emitted UC fluorescence was collected by a lens-coupled monochromator of a 3 nm spectral resolution and with an attached photomultiplier tube. All spectral measurements were performed at room temperature and calibrated by a secondary standard light source. Decay profiles of the 553 and 660 nm radiations were measured by square-wave-modulation of the electric current input to the 976 nm diode laser and by recording the signals via a Tektronix TDS 5052 digital oscilloscope.

3. Results and discussion

The room temperature UC emission spectra of BTO nanocrystals with different Er^{3+} concentrations under 976-nm IR excitation, as shown in Fig. 1, exhibit three distinct bands in the range of 500–700 nm. The bright-green emissions observed between 525 and 553 nm correspond to the $^2H_{11/2} \rightarrow {}^4I_{15/2}$ and $^4S_{3/2} \rightarrow {}^4I_{15/2}$ transitions; the red emission in the 640–680 nm region is assigned to the $^4F_{9/2} \rightarrow {}^4I_{15/2}$ transition. Moreover, Fig. 1 shows the green UC luminescence is distinctly enhanced when the Er^{3+} concentrations changes from 1 mol% to 2 mol%, and the luminescence intensity of the sample doped 2 mol% Er is 2 times higher than that of the sample doped 1 mol% Er. However, as the concentration of Er^{3+} is increased to 3 mol%, we observe an enhancement of the red emission over 1 mol% Er, and there is no change in the green emission. This mainly originates from the enhancement of interionic interactions with increasing the Er^{3+} concentration, inducing the occurrence of the cross relaxation (CR) processes that will be discussed later. Therefore, an optimum Er^{3+} concentration to realize the intense upconverted luminescence is approximately 2.0 mol% in the nanocrystalline BTO host material.

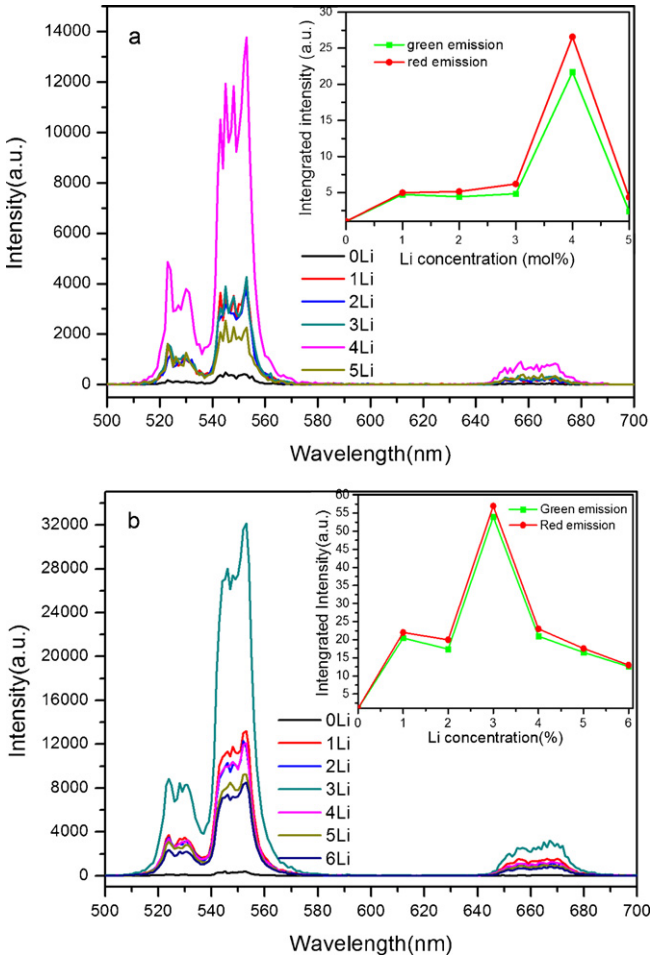

Fig. 2. NIR-to-visible upconversion emission spectra of BTO: 1Er codoped with 1–5 mol% Li^+ ions (a) and BTO: 2Er codoped with 1–6 mol% Li^+ ions (b) under diode laser excitation of 976 nm. The inset is integral intensity of green and red emission as a function of the concentration of Li^+.

In order to understand whether Li^+ ion has sensitize effect to the UC luminescence intensity, BTO doped 1% and 2% Er^{3+} with different concentrations of Li^+ ion were checked. In Fig. 2a, using a fixed Er^{3+} concentration (1 mol%) and upon variation of the Li^+ concentration (from 1 to 5 mol%), it is found that BTO nanocrystals doped with 1 mol% Er^{3+} ions have the weakest emission intensity [20]. Upon increasing the Li^+ concentration, the UC intensity is increased, and it shows a periodic variation. From Fig. 2a (inset), the maximum enhancement presented here is measured to be about 27 times corresponding to Li^+ ions of 4 mol% under same excitation conditions, and the higher incorporation of lithium content cannot enhance the luminescence any more. Such a result is also observed in 2% Er^{3+}-doped BTO nanocrystals. The incorporation of Li^+ ion drastically intensifies the luminescent intensity compared with that of BTO: 2Er (Fig. 2b). When the concentration of Li^+ ion is 3%, the intensity of luminescence is increased up to a factor of 56 times compared with that of lithium free BTO: 2Er (as shown in Fig. 2b (inset)). Furthermore, for BTO: 1Er, we note that the red UC has a larger enhancement times than the green UC by codoping with Li^+ ions.

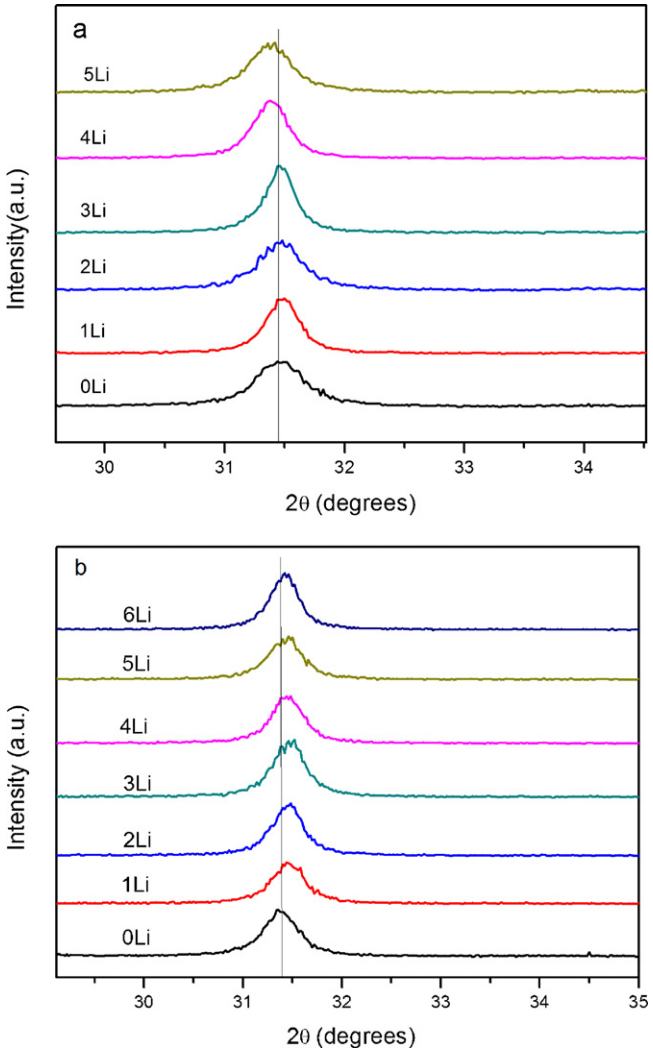

Fig. 3. Measured XRD patterns of peaks (1 1 0) of BTO: 1Er powders codoped with 1–5 mol% Li^+ ions (a) and BTO: 2Er powders codoped with 1–6 mol% Li^+ ions (b).

The XRD patterns of all BTO powders are consisted of cubic phase (JCPDS no. 31-0174) and tetragonal phase (JCPDS no. 05-0626), without any amorphous component and other additional Er_2O_3 crystalline phase. Fig. 3 illustrates the main diffraction peaks (1 1 0) of the 1 mol% Er^{3+}-doped (Fig. 3(a)) and 2 mol% Er^{3+}-doped (Fig. 3(b)) BTO nanocrystals at various Li^+ ion concentrations. On the basis of the XRD patterns, the average sizes of the BTO nanoparticles can be estimated by the Debye–Scherrer's equation:

$$D = \frac{K\lambda}{\beta\cos\theta} \quad (1)$$

where D represents the average diameter of the particles, $K = 0.89$, λ is the wavelength of the CuKα radiation, θ is the Bragg angle, and β is the corrected full width at half-maximum. The strongest peaks (1 1 0) are used to calculate for D of the BTO: Er^{3+} samples with different Li^+ ion concentrations. The calculated results are about 16.7, 22.3, 19.7, 23.9, 22.3, and 19.7 nm for the different samples with Li^+ ion concentrations of 0–5 mol% for the 1% Er^{3+}-doped BTO. The average crystallite sizes of different samples are analogous, which indicates that the particle size has not changed by the introduction of Li^+ ions. This would make a comparison between the luminescence of Er–Li codoped and free Li nanocrystalline materials easily, as the spectroscopy of the nanocrystalline material is particle size dependent. In Fig. 3(a), the main diffraction peaks shift gradually towards larger angles for Li^+ ions of 1–3 mol%, and remain identical after an abrupt turn around to a smaller angle at Li^+ ions of 4 mol%. Li^+ ion is small enough to fit any crystal site, such as substituting the Ba^{2+} ion and occupying the interstitial sites. But, Li^+ ion in the Ti^{4+} site is not likely because of the big charge difference between them. The gradual peak shifts illustrate that Li^+ ions can be doped into the host lattice through the substitution of Ba^{2+} ions below 3 mol%. The constant peak positions for Li^+ ions above 4 mol% suggest that Li^+ ions can occupy the interstitial sites, which cause the host lattice to expand. It is noted that both the substitution of Ba^{2+} ions and the occupation of interstitial sites can tailor the local crystal field around Er^{3+} ions, which is expected to tailor their radiation parameters and affect their anti-Stokes luminescence [18,21].

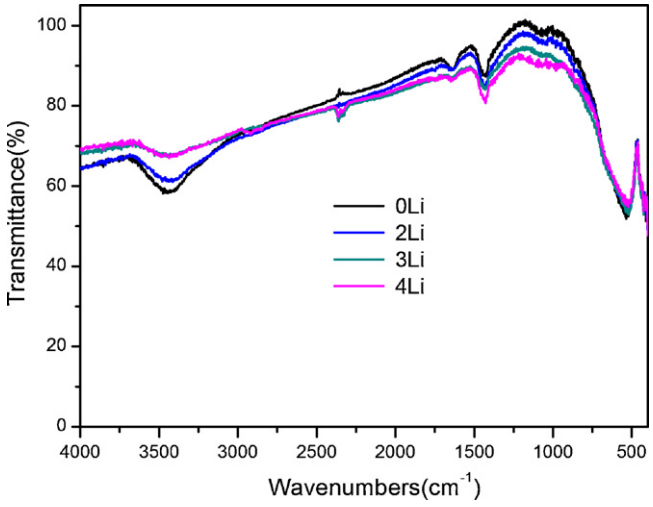

Fig. 4. FT-IR spectra of BTO: 2Er powders codoped with 2–4 mol% of Li^+ ions.

Fig. 3(b) shows diffraction peak positions (1 1 0) of BTO shift to larger angles upon increasing the Li^+ ion concentration to 4 mol%. The calculated crystallite sizes of BTO: 2Er doped with different Li^+ ion concentrations were 19.7, 19.7, 22.3, 20.9, 20.9, 19.7, and 22.3, respectively. The mean distance between the Er^{3+} ions can be estimated by $R = 0.62/(N)^{1/3}$ [11], and the distances between two Er^{3+} ions in BTO: 2Er are shorter than that of in BTO: 1Er. Therefore, the effect of Li^+ on the local asymmetry around Er^{3+} of BTO: 2Er is larger than that of BTO: 1Er, which resulted in a bigger increase times of UC emissions intensities with increasing Li^+ concentration. Furthermore, for the different concentration of Er^{3+}, the Li^+ ion concentration will be different for the distortion of the local asymmetry around Er^{3+}. Tsur et al. [22] has presented that Er occupy A- and B-site and the compensation is mainly via oxygen vacancies. Compared to BTO: 1Er, more Er ions in BTO: 2Er are probably incorporated on the A-site. In this case, two Er ions would substitute for three Ba ions creating a doubly negatively charged vacant Ba site, as shown below [23].

$$Er_2O_3 + 3(Ba_{2+}^{Ba^{2+}})^{\times} = 2(Er_{3+}^{Ba^{2+}})^{\bullet} + (V_{Ba^{2+}})'' + 3BaO$$

More Li^+ ion can be incorporated into BTO lattice both by charge compensation ($(Li_{Ba})' + (Er_{Ba})\bullet$) and by generating oxygen vacancies in the lattice ($2(Li_{Ba})' + (V\ddot{o})$), which leaded to the shrink of the lattice. The distortion of the local asymmetry around Er^{3+} increases, and the transition probabilities which govern various intra-4f-shell transitions of the Er^{3+} ion giving rise to both the green and the red emission increase. As a whole, the enhanced luminescence is conjectured to result from the distortion of the local asymmetry around Er^{3+} and the oxygen vacancy generated by Li^+ ion incorporation in the lattices.

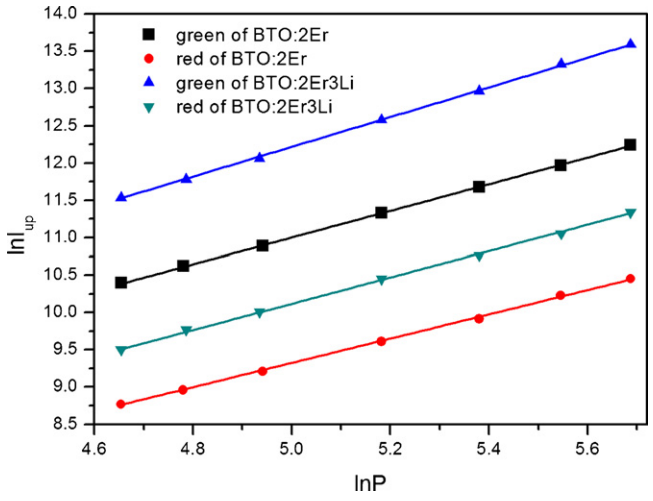

Fig. 5. Pump power dependence of the green and red emission of BTO: 2Er and BTO: 2Er3Li in a logarithmic diagram.

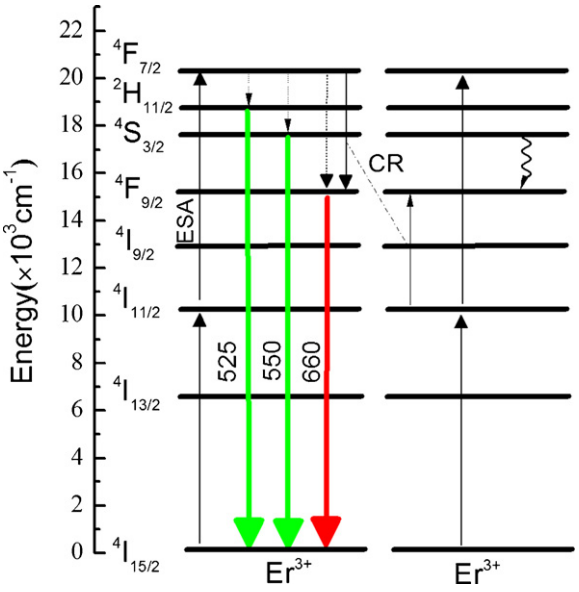

Fig. 6. Energy levels diagram of Er^{3+} ion as well as the proposed UC mechanisms for the green and red emissions.

Fig. 4 shows the FT-IR of BTO: 2Er specimens with different concentration of Li^+ ions. In addition to the absorbance band of Ti–O, the bands occurring at approximately 1430 and 3450 cm^{-1} ascribed to vibrations from the CO and OH groups, respectively, were still observed. It was worthwhile to point out that the absorption bands of the surface contaminants (OH and CO groups) were measured to decrease with the increase of concentration Li^+. It is believed that the OH groups can be neutralized with neighboring Li^+ ions, owing to Coulomb interactions [19,24]. The $^4F_{9/2}$ state is populated via nonradiative decay from the $^4S_{3/2}$ state involving the emission of one high-frequency-vibration phonons to bridge the 3000 cm^{-1} energy gap between the $^4S_{3/2}$ and $^4F_{9/2}$ states [25]. The absorption bands of OH (around 3400 cm^{-1}) became weakest when the concentration of Li^+ ions in BTO: $2Er^{3+}$ specimens were 3% and 4%. Therefore, the multiphonon relaxation rate is weaker than that in other samples, and resulting in observed stronger UC intensity of green emission.

To better comprehend the mechanism(s) which populate the ($^2H_{11/2}$, $^4S_{3/2}$) green- and ($^4F_{9/2}$) red-emitting levels, the upconversion luminescence intensity was measured as a function of the pump power. Fig. 5 shows a logarithmic plot of the integrated emission intensity of the upconverted fluorescence as a function of pump intensity for BTO: 2Er and BTO: 2Er3Li samples. The slopes n obtained for BTO: 2Er were 1.76 ± 0.04 and 1.68 ± 0.02 and for BTO: 2Er3Li were 1.99 ± 0.02 and 1.78 ± 0.02 for green and red emissions, respectively. It is observed that the n-values were enhanced in BTO: 2Er3Li for both green and red emissions [19]. In addition, the n-value for green emissions of $^4S_{3/2} \rightarrow {}^4I_{15/2}$ and $^2H_{11/2} \rightarrow {}^4I_{15/2}$ is reasonably close to 2, while the value of n for the red emission of $^4F_{9/2} \rightarrow {}^4I_{15/2}$ is less than 2 [26]. The slopes of the curve of ln(Intensity) versus ln(Power) were about 2 for both the green and red manifolds and for all samples under investigation. These results indicate that two-photon processes contribute to the green and red UC emissions. As shown in Fig. 6, under the excitation of 976 nm light, Er^{3+} ions are excited initially from the ground state $^4I_{15/2}$ to the $^4I_{11/2}$ state in the ground-state absorption (GSA) process. Following the excited-state absorption (ESA) process, the Er^{3+} ions are further excited to $^4F_{7/2}$ from the $^4I_{11/2}$ state and subsequently decay to the $^2H_{11/2}$ and $^4S_{3/2}$ states. The $^2H_{11/2} \rightarrow {}^4I_{15/2}$ and $^4S_{3/2} \rightarrow {}^4I_{15/2}$ transition gives rise to the green emission in the spectral lines near 525 and 553 nm [27]. It is suggested that a cross-relaxation process is responsible for populating the $^4F_{9/2}$ level and occurs via two resonant transitions: $^4F_{7/2} \rightarrow {}^4F_{9/2}$ and $^4I_{11/2} \leftarrow {}^4F_{9/2}$ between neighboring Er^{3+} ions [28]. The $^4F_{9/2} \rightarrow {}^4I_{15/2}$ transition produces the red emission around 640–680 nm [10]. In fact, cross-relaxation process is the main one populating the $^4F_{9/2}$ level of Er^{3+} in the higher concentration (2–3 mol%) of Er^{3+} doped BTO nanocrystals, giving rise to the enhancement of the red emission, in agreement with the obtained experimental data (Fig. 1). Both Bai et al. [29] and Chen et al. [17], found that in Li–Er codoped Y_2O_3 nanocrystals, the increased times of the red emission were smaller than that of the green emission. In Y_2O_3 nanocrystals, because both Li^+ and Er^{3+} occupy Y^{3+}-site, the cross relaxation (CR) processes involved in the red UC generation are hindered more remarkably. It is worthwhile to mention that smaller intensity enhancement in green emission than in red emission was observed in BTO: 2Er3Li, which arises from the fact that some of the Er^{3+} ions can occupy B-site, while Li^+ only enter into A-site, the reduction of the inter-ionic interaction of Er^{3+} is weaker than Li^+ for Er^{3+} of Y_2O_3.

Fig. 7 shows the measured fluorescence decay of $^4S_{3/2}$ and $^4F_{9/2}$ for BTO: 1Er and BTO: 1Er4Li following excitation with 976 nm laser excitation. It should be pointed out that the decay profiles can best be fitted by a single exponential for all the samples. The

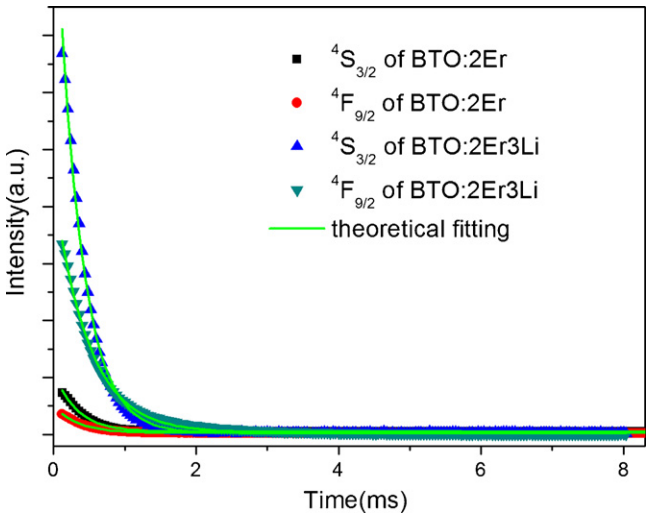

Fig. 7. Decay profiles of $^4S_{3/2}$ (Er) and $^4F_{9/2}$ (Er) for BTO: 2Er and BTO: 2Er3Li under 976 nm laser excitation.

decay time constants $\tau 1$ are 0.281 ms and 0.347 ms for $^4S_{3/2}$ and $^4F_{9/2}$ of BTO: 2Er, and they become 0.299 ms and 0.532 ms for $^4S_{3/2}$ and $^4F_{9/2}$ of BTO: 2Er3Li, respectively. As mentioned above, with Li^+ content changing from 2 to 4 mol%, the amount of high-frequency groups (OH) on the sample surface is decreased. The enhancement of lifetime could be rationally attributed to the decrease of the multiphonon relaxation rate due to the decrease of the amount of OH groups on the BTO: 2Er3Li surface. Furthermore, the distortion of the local asymmetry around Er^{3+} which decreases the nonradiative transition leads to the increase of lifetime of $^4S_{3/2}$ and $^4F_{9/2}$ levels. The decay time constants for BTO: 2Er3Li are considerably longer than that of BTO: 2Er, and more remarkable for red one. The decay time investigation of green and red emissions confirmed directly that the intensity of red emission was changed more remarkably.

4. Conclusions

We provide the report on the enhancement of the infrared-to-visible UC luminescence intensity under the 976 nm laser excitation in Li^+ and Er^{3+} codoped BTO nanocrystals. Significant UC fluorescence enhancements of 27 times from BTO: 1Er4Li than BTO: 1Er and 56 times from BTO: 2Er3Li than BTO: 2Er were observed. The variation of the local structure around Er^{3+} ions results to the change of UC luminescence intensity with codoped different Li^+ in BTO: 1Er and BTO: 2Er. The tailoring effect of Li^+ on the local asymmetry around Er^{3+} of BTO: 2Er is larger than that of BTO: 1Er, which resulted in a bigger increase times of UC emissions intensities with increasing Li^+ concentration. Power-dependence studies of BTO: 2Er3Li suggest that the green ($^2H_{11/2}/^4S_{3/2} \rightarrow {}^4I_{15/2}$) and red ($^4F_{9/2} \rightarrow {}^4I_{15/2}$) UC emissions occurred via a two-photon process. Li^+ ions also can reduce the OH groups in specimens, which is also one reason for enhancing the UC emission intensities.

Acknowledgements

The authors gratefully acknowledge the financial support of Youth Science Foundation of Heilongjiang Province of China (No. QC07C23) and Natural Science Foundation of Heilongjiang Province of China (No. E200905).

References

[1] T. Zako, H. Nagata, N. Terada, M. Sakono, K. Soga, M. Maeda, J. Mater. Sci. 43 (2008) 5325.
[2] N. Rakov, G.S. Maciel, R.B. Guimarães, I.C.S. Carvalho, Mater. Chem. Phys. 123 (2010) 199.
[3] B. Ungun, R.K. Prud'homme, S.J. Budijono, J. Shan, S.F. Lim, Y. Ju, R. Austin, Opt. Express 17 (2009) 80.
[4] C. Xu, Q. Yang, G. Ren, Y. Liu, J. Alloys Compd. 503 (2010) 82.
[5] S. Zeng, G. Ren, Q. Yang, J. Alloys Compd. 493 (2010) 476.
[6] J. Boyer, F. Vetrone, L.A. Cuccia, J.A. Capobianco, J. Am. Chem. Soc. 128 (2006) 7444.
[7] F. Vetrone, J.C. Boyer, J.A. Capobianco, A. Speghini, M. Bettinelli, J. Phys. Chem. B 107 (2003) 1107.
[8] X. Qin, G. Zhou, H. Yang, Y. Yang, J. Zhang, S. Wang, J. Alloys Compd. 493 (2010) 672.
[9] G.Y. Chen, Y.G. Zhang, G. Somesfalean, Z.G. Zhang, Q. Sun, F.P. Wang, Appl. Phys. Lett. 89 (2006) 163105.
[10] T. Huang, W. Hsieh, J. Fluoresc. 19 (2009) 511.
[11] A. Patra, C.S. Friend, R. Kapoor, P.N. Prasad, Chem. Mater. 15 (2003) 3650.
[12] H.X. Zhang, C.H. Kam, Y. Zhou, X.Q. Han, S. Buddhudu, Q. Xiang, Y.L. Lam, Y.C. Chan, Appl. Phys. Lett. 31 (2000) 609.
[13] J. Yang, N. Dai, S. Dai, L. Wen, L. Hu, Z. Jiang, Chem. Phys. Lett. 376 (2003) 671.
[14] F. Vetrone, J.C. Boyer, J.A. Capobiancoa, A. Speghini, M. Bettinelli, Appl. Phys. Lett. 80 (2002) 1752.
[15] A. Patra, C.S. Friend, R. Kapoor, P.N. Prasad, Appl. Phys. Lett. 83 (2003) 284.
[16] J.A. Capobianco, F. Vetrone, J.C. Boyer, A. Speghini, M. Bettinelli, Opt. Mater. 19 (2002) 259.
[17] G. Chen, H. Liu, H. Liang, G. Somesfalean, Z. Zhang, J. Phys. Chem. C 112 (2008) 12030.
[18] G.Y. Chen, H.C. Liu, G. Somesfalean, Y.Q. Sheng, H.J. Liang, Z.G. Zhang, Q. Sun, F.P. Wang, Appl. Phys. Lett. 92 (2008) 113114.
[19] Y. Bai, Y. Wang, K. Yang, X. Zhang, G. Peng, Y. Song, Z. Pan, C.H. Wang, J. Phys. Chem. C 112 (2008) 12259.
[20] M. Yang, Y. Sui, S. Wang, X. Wang, Y. Sheng, Z. Zhang, T. Lü, W. Liu, Chem. Phys. Lett. 492 (2010) 40.
[21] L. Tian, S. Mho, Solid State Commun. 125 (2003) 647.
[22] Y. Tsur, T.D. Dunbar, C.A. Randall, J. Electroceram. 7 (2001) 25.
[23] S. Aggarwal, R. Ramesh, Annu. Rev. Mater. Sci. 28 (1998) 463.
[24] Y. Bai, Y. Wang, G. Peng, K. Yang, X. Zhang, Y. Song, J. Alloys Compd. 478 (2009) 676.
[25] J.C. Boyer, F. Vetrone, L.A. Cuccia, J.A. Capobianco, J. Am. Chem. Soc. 128 (2006) 7444.
[26] Y. Bai, K. Yang, Y. Wang, X. Zhang, Y. Song, Opt. Commun. 281 (2008) 2930.
[27] X. Wang, X. Kong, G. Shan, Y. Yu, Y. Sun, L. Feng, K. Chao, S. Lu, Y. Li, J. Phys. Chem. B 108 (2004) 18408.
[28] F. Vetrone, J. Boyer, J.A. Capobianco, A. Speghini, M. Bettinelli, Chem. Mater. 15 (2003) 2737.
[29] Y. Bai, Y. Wang, G. Peng, W. Zhang, Y. Wang, K. Yang, X. Zhang, Y. Song, Opt. Commun. 282 (2009) 1922.